Environmental Research Letters

LETTER • **OPEN ACCESS**

Inference of the impact of wildfire on permafrost and active layer thickness in a discontinuous permafrost region using the remotely sensed active layer thickness (ReSALT) algorithm

To cite this article: Roger J Michaelides *et al* 2019 *Environ. Res. Lett.* **14** 035007

Environmental Research Letters

LETTER

Inference of the impact of wildfire on permafrost and active layer thickness in a discontinuous permafrost region using the remotely sensed active layer thickness (ReSALT) algorithm

Roger J Michaelides[1], **Kevin Schaefer**[2], **Howard A Zebker**[1], **Andrew Parsekian**[3], **Lin Liu**[4], **Jingyi Chen**[5], **Susan Natali**[6], **Sarah Ludwig**[6] **and Sean R Schaefer**[7]

[1] Department of Geophysics, Stanford University, Stanford, CA 94305, United States of America
[2] National Snow and Ice Data Center, Cooperative Institute for Research in Environmental Sciences, University of Colorado at Boulder, Boulder, CO 80309, United States of America
[3] Department of Geology and Geophysics, University of Wyoming, Laramie, WY 82070, United States of America
[4] Earth System Science Programme, Faculty of Science, The Chinese University of Hong Kong, Hong Kong, People's Republic of China
[5] Department of Aerospace Engineering and Engineering Mechanics, 210 E 24st Street, WRW Building, Austin, TX 78712, United States of America
[6] Woods Hole Research Center,149 Woods Hole Road, Falmouth, MA 02540, United States of America
[7] DePaul University, Chicago IL, 60604, United States of America

E-mail: rmich@stanford.edu

Keywords: permafrost, wildfire, InSAR, radar remote sensing, geophysics, active layer, Arctic

OPEN ACCESS

RECEIVED
20 February 2018

REVISED
10 December 2018

ACCEPTED FOR PUBLICATION
14 December 2018

PUBLISHED
15 March 2019

Abstract

The Yukon–Kuskokwim (YK) Delta is a region of discontinuous permafrost in the subarctic of southwestern Alaska. Many wildfires have occurred in the YK Delta between 1971–2015, impacting vegetation cover, surface soil moisture, and the active layer. Herein, we demonstrate that the remotely sensed active layer thickness (ReSALT) algorithm can resolve the post-fire active layer dynamics of tundra permafrost. We generated a stack of Advanced Land Observing Satellite Phased Array type L-band Synthetic Aperture Radar interferograms over a study region in the YK Delta spanning 2007–2010. We applied ReSALT to this stack of interferograms to measure seasonal subsidence associated with the freezing and thawing of the active layer and subsidence trends associated with wildfire. We isolated two wildfire-induced subsidence signatures, associated with the active layer and the permafrost layer. We demonstrate that InSAR is sensitive to increases in active layer thickness following wildfire, which recovers to pre-fire values after approximately 25 years. Simultaneously, we show that fire gradually thins the permafrost layer by 4 m, which recovers to pre-fire thickness after 70 years.

1. Introduction

Air temperatures in high-latitude regions are increasing at twice the global rate, which threatens the distribution and stability of permafrost regions [1, 2]. Among terrestrial biomes, tundra and boreal ecosystems underlain by permafrost contain the largest below-ground carbon reservoirs globally [3], and these regions are also significantly impacted by wildfires [4, 5]. As air temperatures rise and regional climate changes, wildfires are expected to increase in frequency over the Arctic domain [6, 7]. Under favorable environmental conditions, tundra regions are susceptible to burn [8]. Wildfires rapidly transfer soil and vegetation carbon into the atmosphere. More significantly, post-fire increases in thaw depth facilitate increased microbial decomposition and heterotrophic respiration within the thawed soil column, which gradually releases soil carbon to the atmosphere years after the wildfire event [8–11]. Furthermore, terrestrial arctic regions are thought to contain roughly twice the amount of carbon currently in the atmosphere, so any increases in wildfire frequency in the Arctic could have a marked effect on the global carbon cycle [12].

The maximum annual depth of thaw of surface soils, denoted active layer thickness (ALT), is designated by the World Meteorological Organization as an essential climate variable for monitoring the status of permafrost.

The active layer plays a crucial role in surface processes, surface hydrology, and vegetation succession; as permafrost thaws, decomposition and mineralization of previously frozen carbon can release large stores of carbon into the atmosphere [9, 12]. Fire removes a portion of the insulating organic layer, increasing the ALT for years after the fire [8, 13–15]. Regions with poor drainage, thick organic layers, and fine-grained soil recover rapidly after fire [15]. As the surface vegetation grows back after a fire, the organic layer re-accumulates, and the ALT returns to its pre-fire values [14–16]. However, how long this recovery takes is poorly understood. As wildfire frequency is expected to increase over arctic regions through the 21st century, a more complete understanding of the interaction between wildfire, permafrost, and active layer dynamics is necessary.

In recent years, the remotely sensed active layer thickness (ReSALT) algorithm was developed to study the seasonal subsidence, subsidence trends, and ALT in permafrost regions [17–19]. Soil water expands when it freezes such that soil heaves up in fall when the active layer freezes and subsides in summer when it thaws. ReSALT uses the interferometric synthetic aperture radar (InSAR) technique to measure surface subsidence associated with this freezing and thawing of the active layer. InSAR is a widely-used geophysical technique for measuring surface deformation at high spatial resolution [20]. The ReSALT algorithm has been used to characterize ALT and thermokarst processes across the arctic domain [17–19, 21]. In particular, ReSALT quantified both the increase in seasonal subsidence and melting of massive ground ice on the North Slope of Alaska due to the 2007 Anaktuvuk fire [21, 22]. However, the dynamics of post-fire response of the active layer and permafrost column remain poorly understood.

The Yukon–Kuskokwim (YK) Delta is a subarctic lowland in the discontinuous permafrost zone dotted with lakes, thaw ponds, and wetlands [23]. The YK Delta represents an ecologically-driven permafrost system where vegetation dynamics control the formation of permafrost. Vegetation such as moss and grass and the surface layer of organic material thermally insulate the soil in summer, allowing the build up of a permafrost layer and controlling ALT [15, 24]. Major wildfires have burned across the YK Delta many times over the last hundred years. We focused on a wetland tundra region within the Izaviknek Highlands approximately 80 km northwest of Bethel, Alaska that has experienced more than 20 distinct wildfires since 1971 (figure 1). We leveraged the high density of fire scars of various ages to study ALT and permafrost thickness response after fire using the ReSALT algorithm.

2. Methods

2.1. InSAR processing

Using 8 repeat pass ALOS PALSAR FBS (wavelength $\lambda = 23.6$ cm) scenes acquired between 08/12/2007–01/02/2010, we generated a stack of coregistered interferograms over the YK Delta study region using the motion-compensation processing algorithm developed in the Stanford Radar Group [25]. We used the 5 m resolution optical stereophotogrammetric ArcticDEM dataset to remove the topographic phase term from all interferograms. Interferograms were multilooked for increased signal-to-noise ratio at the expense of spatial resolution, and a Goldstein filter was applied to smooth out interferogram phase noise and aid in phase unwrapping [26]. Interferograms were then unwrapped using the Snaphu algorithm described in [27], and deramped to remove the best fit first-order orbital phase error [28]. Individual interferograms corrupted by ionospheric noise or severe surface decorrelation were removed from the stack (see appendix B1 for a table of interferograms used in the final analysis). As InSAR measures deformation in the line-of-sight (LOS) direction of the radar, an LOS correction was applied to all interferograms to decompose the deformation values into horizontal and vertical orientations [28]. We masked consistently incoherent pixels from which precise deformation measurements cannot be retrieved, which masked out major lakes and waterbodies in the study region. As a reference point, we chose an unburned location (61.354 4° N,163.091 1°W; near site 2 in figure 1) where we measured ALT *in situ* in 2016 and then applied our frozen soil expansion model to determine the absolute phase differences within the InSAR stack [18, 19].

We applied the ReSALT algorithm (described below; see A1 for a diagrammatic representation) on the 14 interferograms listed in appendix B1. These interferograms encompass scenes from the onset and end of summer thaw, as well as winter freeze-up. In general, the use of more interferograms will result in a more robust solution. Because snow cover is uncorrelated with time between winter-summer and multiple year winter scene pairs, we retain interferograms containing a winter scene that exhibit surface correlation comparable to summer–summer interferograms. Compared to the ALOS satellite, surface decorrelation is more severe for interferograms generated by the ERS-1 and ERS-2 satellites due to their longer temporal baselines and relatively shorter wavelength ($\lambda \approx 5$ cm versus $\lambda \approx 23$ cm). For this reason previous applications of the ReSALT algorithm have discarded winter scenes to avoid the potential for misinterpreting spurious signals associated with snow cover [17, 18]. The longer wavelength ($\lambda \approx 23$ cm) and shorter temporal baseline of the ALOS PALSAR system used in this study both mitigate surface decorrelation associated with winter snow cover, though we note that their inclusion is a potential source of uncertainty.

2.2. ReSALT retrieval algorithm

The ReSALT algorithm estimates seasonal subsidence, subsidence trends, and ALT from remotely sensed measurements of surface deformation. We include a brief summary here for clarity, and refer readers to

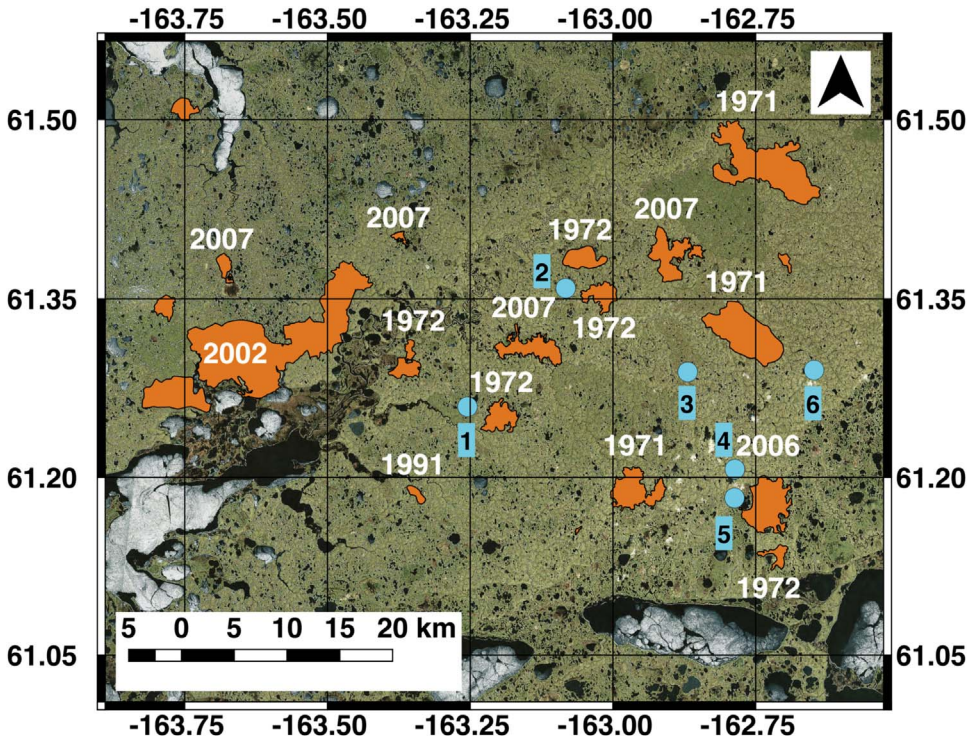

Figure 1. The YK Delta field study area. Wildfire burn zones are shown in orange and labeled by year of burn. Blue dots are the locations of field camps from the 2016 field campaign; *in situ* measurements of thaw depth were made around these sites, characterizing both unburned and burned regions in nearby fire scars (e.g. the 2006 fire adjacent to site 5 and the 2007 fire adjacent to site 2).

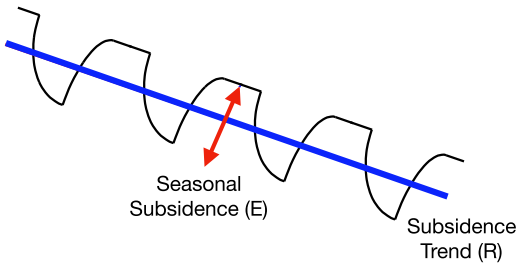

Figure 2. Deformation is decomposed into seasonal subsidence (E) due to seasonal freezing/thawing of the active layer, and long-term trends in subsidence (R) due to thinning of permafrost or thermokarst.

[18, 19] for a detailed description. The ReSALT subsidence model consists of seasonal subsidence and frost heave superimposed on a subsidence trend (figure 2) . As the active layer thaws, ice in the soil undergoes a phase change to liquid water, decreasing in volume and causing the ground to subside [18]. Conversely, when the soil freezes in autumn and early winter, water in the soil changes to ice and the ground heaves. When the active layer freezes completely in mid-winter, the heave stops. Thawing from the top down, the thaw depth increases over time during summer as the square root of cumulative degree days of thawing, as shown by both observations and theory [18, 19]. Conversely, frost heave in autumn follows the square root of degree days of freezing. Seasonal subsidence (E) is the ground height in winter minus the height at maximum thaw at the end of summer and R is the linear trend in subsidence.

The ReSALT deformation model results in a set of linear equations for E, R and ϵ_{topo} a topographic error term that accounts for errors in the digital elevation model [21]. This equation can be expressed in matrix form as:

$$\begin{bmatrix} \delta\phi_1 \\ \cdot \\ \cdot \\ \delta\phi_N \end{bmatrix} = \begin{bmatrix} t_{2,1} - t_{1,1} & \sqrt{\text{ADDT}_{2,1}} - \sqrt{\text{ADDT}_{1,1}} & B_{perp,1} \\ \cdots & \cdots & \cdots \\ \cdots & \cdots & \cdots \\ t_{2,N} - t_{1,N} & \sqrt{\text{ADDT}_{2,N}} - \sqrt{\text{ADDT}_{1,N}} & B_{perp,N} \end{bmatrix} \begin{bmatrix} R \\ E \\ \epsilon_{topo} \end{bmatrix}, \quad (1)$$

where $\delta\phi_i$ terms are InSAR measurements of surface deformation (cm) for the ith interferogram, $t_{2,i} - t_{1,i}$ are the differences in time between any two

scenes used to generate the ith interferogram, $\sqrt{\text{ADDT}_{2,i}} - \sqrt{\text{ADDT}_{1,i}}$ are the differences in the square root of the accumulated degree days of thaw between the two scenes used to generate the ith interferogram, and B_{perp} is the spatial baseline of the ith interferogram. These deformation components represent, respectively, long-term trends in subsidence (R (cm yr^{-1}); specifically associated with wildfire burn in this study), deformation associated with the seasonal freezing/thawing of the active layer (E (cm)), and an error term associated with errors in the digital elevation model used (ϵ_{topo}); see figure 2 for an illustration of the difference between the seasonal subsidence and the subsidence long-term trend. ADDT is calculated from available air temperature records at Bethel, Alaska, normalized such that the maximum value is one at the end of the thaw season [18]. The ReSALT algorithm solves for E, R, and ϵ_{topo} on a pixel-by-pixel basis using least-squares regression. This technique represents a modification of the small baseline subset algorithm originally formulated in [24] and used extensively in InSAR time series analysis [29–32]. Uncertainty is the root mean square error of the differences between the subsidence model and deformations from the interferogram stack [18, 19, 33].

ReSALT estimates ALT from seasonal subsidence E using a model of frozen soil expansion:

$$E = \frac{\rho_w - \rho_i}{\rho_i} \int_0^{\text{ALT}} PS dz, \qquad (2)$$

where P is soil porosity (m^3 m^{-3}), S is soil moisture fraction of saturation (−), z is depth (m), ρ_w is the density of water (kg m^{-3}), and ρ_i is the density of ice (kg m^{-3}) [18, 19]. We assume organic content and thus P decrease exponentially with depth from pure organic to pure mineral soil [18]. S represents the fraction of soil pore space filled with water and is safely assumed to be fully saturated soil on the YK Delta ($S = 1$). ALT is calculated using numerical integration, and uncertainty in ALT is estimated using Gaussian error propagation of uncertainty in E [18].

2.3. Fire response model

Fire increases ALT by removing insulating organic matter from the surface (figure 3). Grass, moss and dead organic matter build up over time to create an organic layer that insulates the soil from warm summer air temperatures, thereby lessening seasonal thaw. Black soot increases absorption of sunlight and fire removes part of the organic layer, resulting in deeper summer thaw and larger ALT, and the potential for thinning of permafrost at depth. Rapid vegetation regrowth after a fire eliminates the albedo effect, but recovery of the organic layer takes many years [34]. As the organic layer becomes thicker, its insulating effect increases and the ALT recovers back to pre-fire conditions [15].

We used the ReSALT output to create a fire response model of seasonal subsidence and permafrost thickness. We assumed post-fire variations in the seasonal subsidence result from variations in ALT, while variations in subsidence trends result from changes in permafrost thickness. Thermokarst subsidence is minimal in the YK Delta because the soil contains very little excess ground ice in the form of ice wedges or layers [24, 35]. Satellite imagery shows the 2007 fires occurred several months before the first ALOS scene, so all the fires in the study region occurred before the ALOS record.

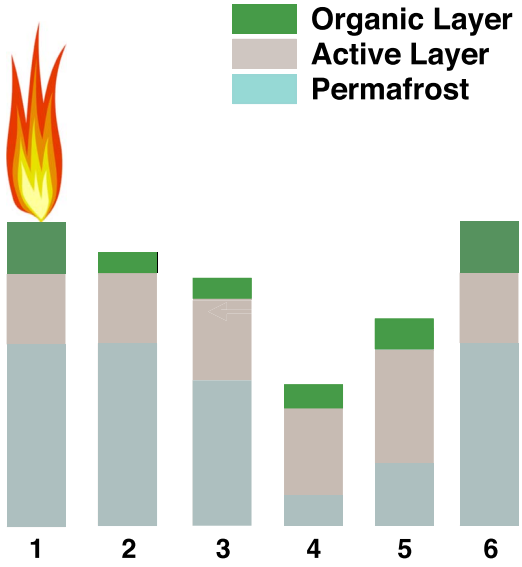

Figure 3. A schematic of fire response in permafrost [15]. (1) Fire removes vegetation and part of the surface organic layer. (2) The removal of the insulating organic layer and change in albedo surface increases energy into the soil. (3) The ALT increases over several years. (4) ALT reaches a maximum. (5) The organic layer gradually thickens as a result of vegetation growth and the ALT decreases. (6) The permafrost system returns to pre-fire conditions.

To create a general permafrost thickness and ALT response model, we performed a 'space for time swap' assuming variations in seasonal subsidence and subsidence trends in burn scars result solely due to variations in time since initial burn. This implicitly assumes that all areas burned exhibit an identical fire response. We calculated the mean ReSALT estimates of seasonal subsidence, subsidence trend, ALT, and their associated uncertainties within each fire zone, yielding 13 estimates of post-fire seasonal subsidence and subsidence trend for 6 different points in time. We applied a student's t-test at 95% significance to determine if values within the fire scars show a significant difference to values outside the scars. We generated two general response functions by sampling the subsidence trend and seasonal subsidence of each fire scar at its respective time since burn, spanning 1971–2007. We performed a nonlinear least-squares best fit to the subsidence trends with a simple quadratic model of fire response:

$$R_{fire}(t) = a_1 e^{b_1 t} + c_1, \qquad (3)$$

where R_{fire} (cm yr^{-1}) is fire response subsidence trend, and a_1, b_1, and c_1 are empirical coefficients. Integrating equation (4) gives the subsidence response associated

with R_{fire}:

$$D_{fire}(t) = \int_0^t R_{fire}(\tau)d\tau = \int_0^t (a_1 e^{b_1 \tau} + c_1)d\tau, \quad (4)$$

where D_{fire} (cm) is the fire response subsidence associated with the D_{fire}. Similarly, we estimated the fire response of seasonal subsidence with a nonlinear least-squares fit to a model of the form:

$$E_{fire}(t) = a_2 e^{b_2 t} + c_2 t + d_2, \quad (5)$$

where E_{fire} (cm) is the fire response in seasonal subsidence, and a_2, b_2, c_2, and d_2 are empirical coefficients that determine the quadratic response of the seasonal subsidence as a function of time. This function corresponds to the integral of the subsidence trend model in equation (4) so that we can compare E_{fire} and D_{fire}. Because E only correlates with recent burns, we fit equation (6) to fire burns from 1991–2007, as the seasonal subsidence of older fires is statistically indistinguishable from unburned permafrost (see results). For both response functions, we calculate the two-norm of the residuals from the least-squares solution, the two-norm of the data uncertainty, and treat these two error sources as dependent uncertainties.

2.4. Field validation and calibration

We validated the ReSALT estimates of ALT with field measurements from a 2016 summer field campaign. The standard technique for measuring ALT in the field is by mechanical probing of the active layer [36]. In addition, we employed field geophysical instruments such as ground-penetrating radars (GPRs) to image the permafrost table, which exhibits a sharp discontinuity in dielectric constant [37]. We collected probing measurements and GPR transects in late August based out of 6 sites within the study region (figure 1). From these sites, we sampled 2006 and 2007 burn scars and unburned tundra by dragging the GPR along the tundra surface [19]. A total of 24 km of GPR transect data was collected, encompassing approximately 12 km of data over burned and unburned tundra each. We made contemporaneous calibration probing measurements to estimate radar velocities, from which the ALT can be directly estimated from the two-way travel time of the radar. For calibration of ReSALT, we chose field measurements made in areas unaffected by wildfire, under the assumption that these unburned regions appear stable over the time period of interest. To assess the agreement between the ReSALT and GPR ALT values, we averaged all GPR traces within a single ReSALT pixel, and compared the absolute value difference between the GPR and ReSALT measurements using the χ^2 statistic [19]:

$$\chi^2 = \left(\frac{\mathrm{ALT_{ReSALT}} - \mathrm{ALT_{GPR}}}{\epsilon_{\mathrm{GPR}}}\right)^2, \quad (6)$$

where $\mathrm{ALT_{GPR}}$ is the *in situ* ALT measured by GPR, $\mathrm{ALT_{ReSALT}}$ is the ReSALT-estimated ALT, and ϵ_{GPR} is the uncertainty in $\mathrm{ALT_{GPR}}$. An ideal match occurs when $\chi^2 < 1$, indicating ReSALT and GPR values agree within uncertainty and are statistically identical. A good match occurs when the uncertainty bars overlap ($1 < \chi^2 < 2$). A poor match occurs when the uncertainty bars do not overlap ($\chi^2 > 2$). Variation within these categories has no physical meaning: a χ^2 of 0.5 is not better than 0.9, since both are statistically identical.

3. Results

ReSALT measurements reveal a complex history of the effects of wildfires on permafrost and active layer dynamics. Fire zones appear as spatial anomalies in subsidence trends that are statistically significantly different from the surrounding, undisturbed tundra with low or uniform subsidence trends (figure 4(a)). Recent fires exhibit large positive subsidence trends corresponding to subsidence while older fires exhibit negative subsidence trends corresponding to uplift. This pattern appears consistent with a post-fire phase of permafrost degradation and thinning, followed by a more gradual recovery phase. The spatiotemporal correlation of the subsidence trends with wildfire scars suggests that the transitory effect of wildfire on permafrost can induce thinning of permafrost for decades after the fire, and that we can measure this signal with ReSALT. The subsidence trends within fire scars compare favorably to rates of permafrost degradation estimated by Schur and Jorgenson in a disturbed ecosystem-driven permafrost system [15]. Additionally, the response appears consistent with modeling efforts to understand the effect of wildfire on permafrost in lowland boreal forests [38]. Subsidence trends for an ecosystem-driven permafrost region in thermal equilibrium are expected to be small [15].

The seasonal subsidence shows a characteristic pattern corresponding to raised peat plateaus and separated by thermokarst gullies (figure 4(c)). In general, the gullies have larger seasonal subsidence than the peat plateaus due to higher water content. The peat plateaus appeared uniformly flat and raised above the gullies by about three meters. The thickness of permafrost in the YK delta was previously estimated to be 10 m under 1 m peat plateaus, assuming a soil column of water ice [39]. We observed peat plateaus ranging from 1–3 m in height, which is consistent with soil expansion of 25–74 m of permafrost (equation (2), $P = 0.45$ for a typical silty soil). However, we typically could not detect the permafrost table with the metal probes or GPR within the gullies indicating no permafrost at all or the presence of a thick layer of unfrozen soil known as a talik. Essentially, we see permafrost under the peat plateaus and no permafrost in the gullies. ReSALT readily detects seasonal subsidence due to active layer thaw over permafrost on the plateaus and due to freezing of surface soils in non-permafrost soils in the gullies.

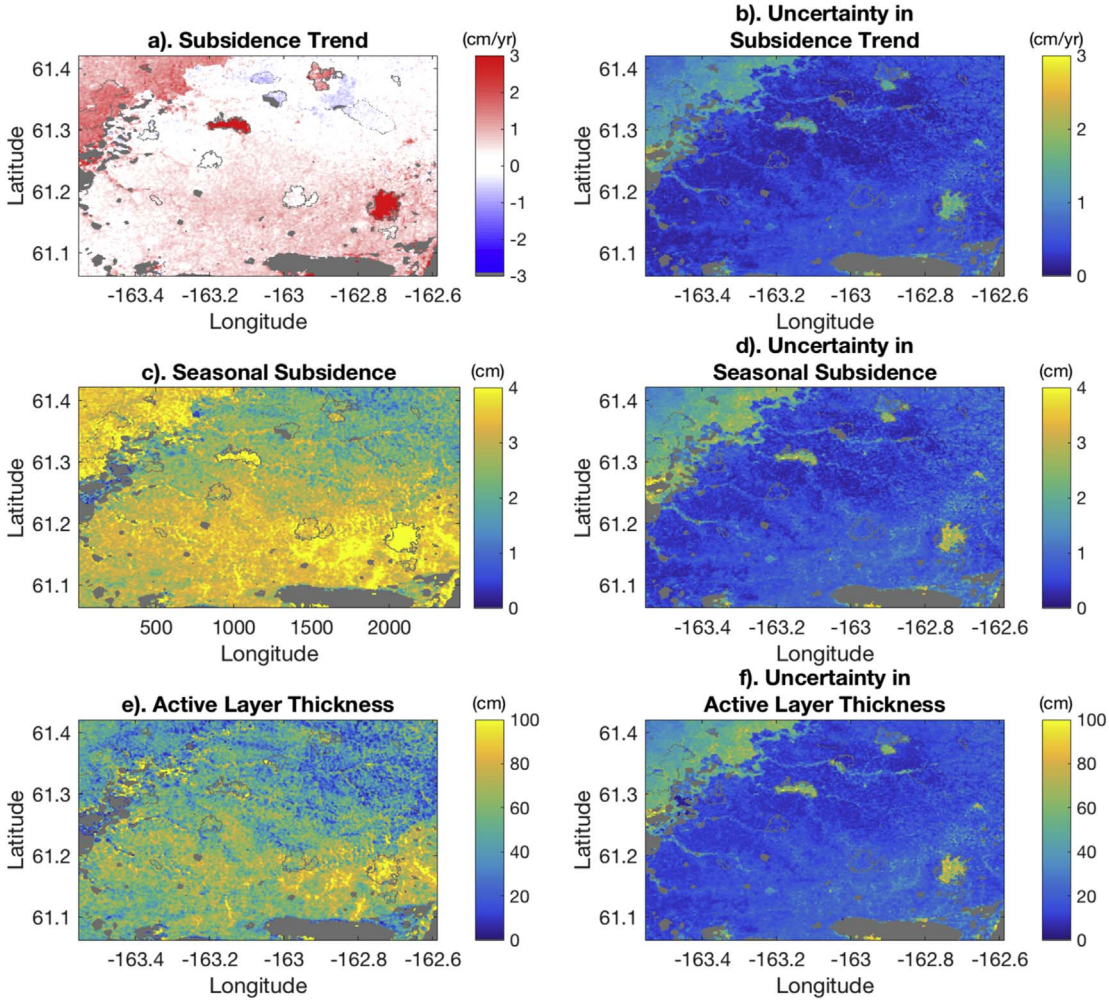

Figure 4. Results from application of the ReSALT algorithm to the YK study region. (a) ReSALT-derived long-term subsidence trend, positive values correspond to an increase in thaw depth (cm yr^{-1}). (b) Uncertainties in long-term trends. (c) ReSALT-derived average seasonal subsidence from 2007–2010 (cm yr^{-1}). (d) Uncertainties in seasonal subsidence. (e) ReSALT-derived ALT (cm). (f) Uncertainties in ALT (cm). Of particular note are the large positive trends in recent burn areas from the 2000s, and negative trends in regions that were burned in the 1970s. Wildfires are outlined in gray, and a red box surrounds the fire scar discussed in figure 5.

Like in *R*, the fire scars also appear as spatial anomalies in seasonal subsidence. The most recent fires show large, statistically significant differences with the surrounding, undisturbed tundra. However, the oldest fires show seasonal subsidence statistically identical to their unburned surroundings. This suggests wildfire has a more transient effect on seasonal subsidence than subsidence trends.

ALT shows the same mottled pattern as the seasonal subsidence, with larger values in the gullies and smaller values on the plateaus (figure 4(c)). However, our field measurements indicate no permafrost in the gullies. What ReSALT measures as ALT in the gullies actually represents the thickness of the seasonally frozen surface layer in non-permafrost soil. Like the seasonal subsidence, we see statistically significant spatial anomalies in the more recent fires, but not for the oldest fires, suggesting ALT recovers from wildfires quicker than subsidence trends.

Comparison of ReSALT and GPR measurements of ALT yields ideal matches for 53% of the data and good matches for 13% of the data (figure 5). An ideal match indicates the ReSALT and GPR values are statistically identical and a good match indicates the uncertainty bars overlap. ReSALT and GPR agreed in the unburned tundra, but not in the 2007 fire zones. The ALOS data starts immediately after the 2007 fire so that the interferogram stack reflects the pre-recovery stage of the fire response model (steps 1–3 of figure 3) [14]. We made the GPR measurements in 2016, nine years after fire and reflecting the last stages of fire recovery of the active layer. The ReSALT ALT shows a positive bias relative to GPR values in the 2007 fire zone, consistent with nine years of recovery after the fire.

The incorporation of scenes from either outside the thaw season, or in the uplift season may necessitate a more physically realistic model of seasonal subsidence than the one used in this work, as noted in. Recently, Hu *et al* introduced a composite index that encapsulates both the thaw subsidence and freeze uplift of permafrost, and demonstrated agreement with GPS reflectometry data [40]. Modifying the

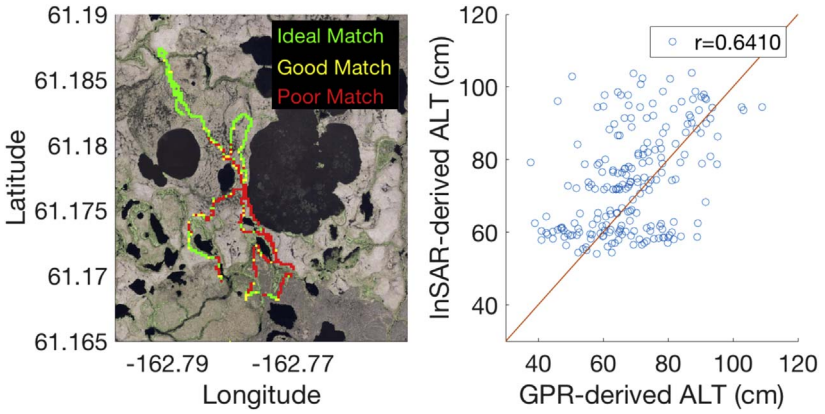

Figure 5. Comparison between GPR and InSAR estimates of ALT at site 5. Left: total path of GPR, color coded based upon the result of the χ^2 test. Right: correlation between the GPR and InSAR estimates of ALT, $r = 0.6410$. Both techniques capture fine spatial variability of ALT and yield mutually consistent results in unburned tundra, while there is little agreement in the region affected by the 2006 fire (bottom half of the survey).

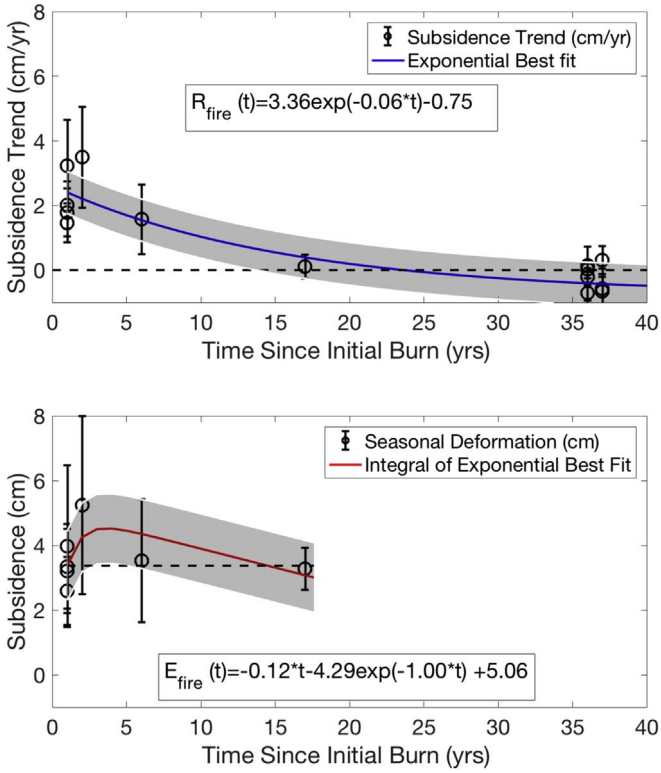

Figure 6. Top: exponential best fit to subsidence trends, exhibiting an increase in permafrost thinning for the first two decades after fire, followed by a more gradual thickening as the permafrost slowly reforms. Dotted line represents 0 subsidence trend; the intersection of the subsidence trend with the 0 trend line corresponds to the beginning of permafrost recovery. Bottom: Integral-Exponential best fit to seasonal subsidence, exhibiting an increase in seasonal thaw depth for the first decade after fire, and a total recovery of approximately 16 years. Dotted line corresponds to a pre-fire seasonal subsidence of 3 cm.

ReSALT algorithm to consider both freezing and thawing indices is the subject of future work. Additionally, large seasonal variations in volumetric water content and saturation can be falsely interpreted as deformation signals [38]. Incorporation of independent observations of soil moisture into the ReSALT algorithm is an important piece of future work, as the ReSALT algorithm does not currently take into consideration spatial or temporal variability of volumetric water content. In general, the use of more interferograms leads to more robust solutions with the ReSALT algorithm. The launch of the NiSAR mission in 2021 will allow for the collection of L-band ($\lambda \approx 23$ cm) SAR imagery suitable for InSAR at 6–12 d repeat intervalsa significant improvement to the repeat interval of the ALOS satellite. This will allow

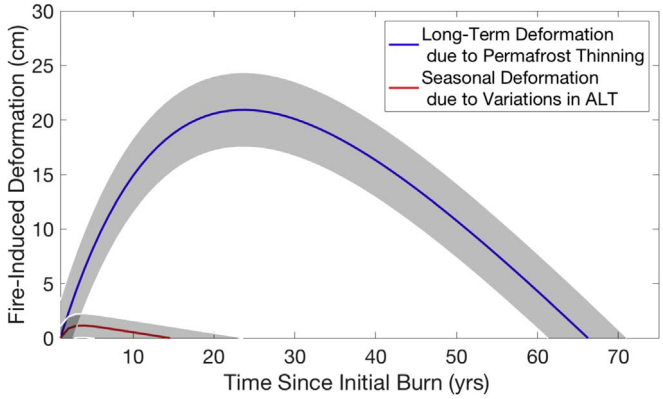

Figure 7. Comparison of the best-fitting seasonal subsidence (equation (3); red) and the integrated subsidence trend (equation (5); blue) induced by wildfire, with their associated uncertainties in gray. These deformations are associated with, respectively, variations in the seasonal thaw depth of the active layer, and thinning of permafrost. These two processes occur over 15 ± 7 years, and 66 ± 5 years, respectively.

for more accurate characterization of the seasonal subsidence and subsidence trends of permafrost regions.

Our fire response models indicate seasonal subsidence and ALT recover much faster than subsidence trends after a fire (figure 6). The seasonal subsidence response appears consistent with a previous study of post-fire active layer dynamics in the Canadian tundra [14]. Immediately after a fire, the seasonal subsidence experiences a gradual increase for approximately a decade reflecting deeper seasonal thaw depths. The seasonal subsidence then reverses sign as the organic layer gradually re-accumulates and the thaw depth decreases [8, 14, 15]. After 15 years, the seasonal subsidence returns to its pre-fire thermal equilibrium. As expected, ALT reflects seasonal subsidence and returns to pre-fire values after 15 years (not shown). In contrast, subsidence trends show a much longer response, changing from positive to negative at 25 years, indicating a change from subsidence to heave, and eventually returning to zero after 65–70 years.

4. Discussion

ReSALT measures two separate, but related responses to fire: active layer thickening and permafrost thinning (figure 7). The integral of the subsidence trend response model (equation (5)) represents the impact of fire on permafrost thickness. The seasonal subsidence response model represents the impact of fire on the thickness of the active layer. The removal of vegetation and organic material by fire increases energy absorption by the ground, which will increase ALT, seasonal subsidence, and the permafrost temperature. The thickness of permafrost balances freezing from the surface and warming from the Earth's interior, so any increase in permafrost temperature would result in a thinning of the permafrost layer.

Both fire response models show two distinct phases: a perturbation phase and a recovery phase. Both response curves start at zero, which represents pre-fire thermal equilibrium conditions. In the perturbation phase, the subsidence increases from zero to a maximum value. In the recovery phase, the subsidence slowly decreases back to zero or pre-fire conditions. Both response models show a recovery phase approximately twice as long as the perturbation phase.

Fire increases the thickness of the active layer, resulting in an increase in seasonal subsidence. The perturbation phases lasts ≈5 years and peaks at 1.7 cm, which, using our soil expansion model, corresponds to a 26 cm increase in ALT. The ALT response model shows consistent results (not shown). The vegetation grows back quickly, eliminating the albedo effect and stopping the increase in ALT after ≈5 years. This appears consistent with the rapid post-fire vegetation regrowth associated with tundra fires [41]. In the recovery phase, which lasts ≈10 years, the vegetation and organic layer thicken, insulating the soil and decreasing ALT and seasonal subsidence. After 15 ± 7 years, the organic layer returns to per-fire conditions, along with ALT and seasonal subsidence.

Fire raises the temperature of the permafrost layer, thinning the permafrost layer [8]. A warm temperature anomaly introduced at the surface takes years to propagate downward throughout the soil column [42]. The subsidence response model peaks at 20 cm about 25 years after a fire. If we assume this susbsidence is describable entirely by the soil physics model we have employed, for an initial permafrost thickness of 25 m of saturated silty soil with a porosity of 45%, 20 cm of subsidence corresponds to a thinning of the permafrost by ≈5 m, or 20%. Such subsidence cannot result from increases in active layer thaw depth, which would correspond to an increase in ALT of ≈5 m, which we do not observe. Some of this subsidence may be due to soil compaction, for which our soil physics model does not account. These estimates of permafrost thinning thus represent an upper bound estimate.

The permafrost thinning response depends on the seasonal subsidence response, but takes approximately five times longer. The seasonal subsidence and ALT response depends on energy balance in the summer, but the permafrost thinning depends on annual energy balance. The permafrost thinning cannot peak until the seasonal subsidence and ALT peak, but lags due to the time required to propagate temperature anomalies. As a result, seasonal subsidence and ALT peak after 5 years, but permafrost thinning peaks after 25 years. Seasonal subsidence and ALT return to pre-fire conditions after 15 ± 7 years, but permafrost thickness returns to pre-fire conditions after 66 ± 5 years.

Our results emphasize the importance of ecological processes in controlling permafrost dynamics, where local vegetation plays a significant role in the thermal insulation of permafrost and the post-fire response [15, 43]. Removal of surface vegetation and a fraction of the overlying organic layer of the active layer by wildfire modifies the thermal insulation and albedo of the surface, making permafrost susceptible to a deeper seasonal thaw depth. In areas with a thick organic layer, poor drainage and fine-grained soil, the permafrost system can eventually return to its pre-fire equilibrium state, or reach a new thermal equilibrium [41]. This response is driven by the gradual re-accumulation of an organic layer as a by-product of the ecological regrowth of the surface vegetation, which insulates the permafrost and gradually decreases the seasonal thaw depth of the active layer [15, 44]. Simultaneously, wildfires induce a thinning of permafrost; the recovery time scales between active layer and permafrost differ by almost a factor of five, and thickening of the permafrost is first contingent upon the total recovery of the active layer. Post-fire active layer dynamics are different in different permafrost regimes, such as black spruce forests, where fire can initiate irreversible permafrost degradation [15, 45]. However, as a demonstration of technique, we illustrate that ReSALT can successfully infer and discriminate between post-fire permafrost and active layer dynamics of permafrost. In the future, this technique should be extended to other regions under different permafrost and climatic regimes to further constrain post-fire permafrost active layer dynamics as a function of permafrost regime and fire severity.

5. Conclusions

Fire in the YK Delta increases seasonal subsidence and ALT while simultaneously thinning the permafrost layer. We applied the ReSALT algorithm to the YK Delta to estimate seasonal subsidence, subsidence trends, ALT, and uncertainties. ALT ranges from 10–120 cm, and correlates with surface geomorphology. We compared the ReSALT and GPR measurements of ALT agree for 68% of the pixels, with higher agreement in undisturbed tundra than in fire zones. Using burn scars and fire ages, we constructed fire response models. Seasonal subsidence and ALT response to fire peaks at 5 years and returns to pre-fire conditions after 15 ± 7 years. The peak seasonal subsidence response is 1.7 cm corresponding to an increase in ALT of 26 cm. The permafrost thins in response to fire, with a peak at 25 years and a recovery to pre-fire conditions after 66 ± 5 years. The peak subsidence associated with permafrost thinning was 20 cm, corresponding to a thinning of the permafrost layer by 5 m.

Acknowledgments

This material is based upon work supported by the National Science Foundation Graduate Research Fellowship under Grant No. DGE1656518, NASA Grant NNX16AH36A, Hong Kong Research Grants Council CUHK14300815, Geophysical instrumentation used in this study was supported by NSF EPSCoR award #1208909, InSAR data was provided by the Alaska Satellite Facility (ASF), DEMs provided by the Polar Geospatial Center under NSF OPP awards 1043681, 1559691 and 1542736. This study was part of the Arctic-Boreal Vulnerability Experiment.

Appendix A.

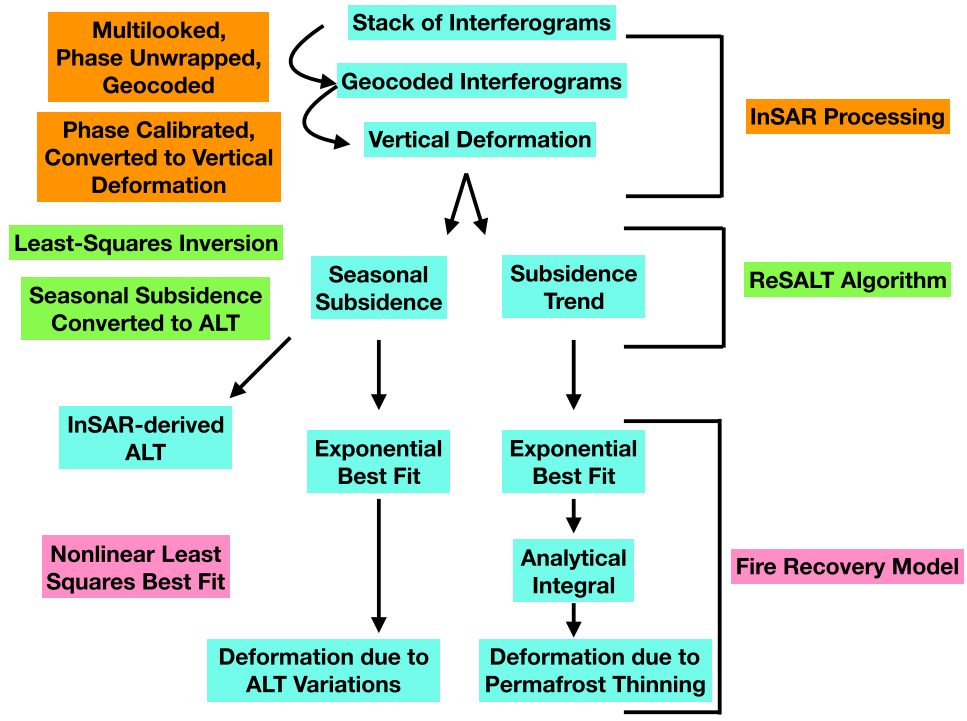

Figure A1. Diagram of processing applied to InSAR data as described in the Methods. Data at various levels of processing are in blue; processing steps described in 3.1 are in orange; Processing steps described in 3.2 are in green; processing steps described in 3.3 are in pink.

Appendix B.

Table B1. InSAR scene pairs used in this study.

Interferogram #	Date 1	Date 2	Scene 1	Scene 2	Time span (days)	Perpendicular baseline (m)
1	20070812	20070927	ALPSRP082461220	ALPSRP089171220	46	389
2	20070812	20071228	ALPSRP082461220	ALPSRP102591220	138	2514
3	20070812	20080814	ALPSRP082461220	ALPSRP136141220	368	−5003
4	20070812	20100102	ALPSRP082461220	ALPSRP209951220	874	−27
5	20070927	20071228	ALPSRP089171220	ALPSRP102591220	92	1544
6	20070927	20100102	ALPSRP089171220	ALPSRP209951220	828	−997
7	20071228	20080212	ALPSRP102591220	ALPSRP109301220	46	1034
8	20071228	20081230	ALPSRP102591220	ALPSRP156271220	368	−4408
9	20071228	20090214	ALPSRP102591220	ALPSRP162981220	414	−3527
10	20071228	20100102	ALPSRP102591220	ALPSRP209951220	736	−1137
11	20080212	20100102	ALPSRP109301220	ALPSRP209951220	690	−2171
12	20081230	20090214	ALPSRP156271220	ALPSRP162981220	46	881
13	20081230	20100102	ALPSRP156271220	ALPSRP209951220	368	3271
14	20090214	20100102	ALPSRP162981220	ALPSRP209951220	322	2390

ORCID iDs

Roger J Michaelides https://orcid.org/0000-0002-7577-6829
Andrew Parsekian https://orcid.org/0000-0001-5072-9818
Lin Liu https://orcid.org/0000-0002-9581-1337

References

[1] Jorgenson M T, Racine C H, Walters J C and Osterkamp T E 2001 Permafrost degradation and ecological changes associated with a warming climate in central Alaska *Clim. Change* **48** 551–79
[2] Osterkamp T E, Jorgenson M T, Schuur E A G, Shur Y L, Kanevskiy M Z and Vogel J G 2009 Physical and ecological changes associated with warming permafrost and thermokarst in interior Alaska *Permafrost Periglacial Process.* **20** 235–56
[3] Hugelius G *et al* 2014 Estimated stocks of circumpolar permafrost carbon with quantified uncertainty ranges and identified data gaps *Biogeosciences* **11** 6573–93
[4] Loranty M M, Lieberman-Cribbin W, Berner L T, Natali S M, Goetz S J, Alexander H D and Kholodov A L 2016 Spatial variation in vegetation productivity trends, fire disturbance, and soil carbon across arctic-boreal permafrost ecosystems *Environ. Res. Lett.* **11** 095008
[5] Genet H *et al* 2013 Modeling the effects of fire severity and climate warming on active layer thickness and soil carbon storage of black spruce forests across the landscape in interior Alaska *Environ. Res. Lett.* **8** 045016
[6] Hinzman L D *et al* 2005 Evidence and implications of recent climate change in Northern Alaska and other Arctic regions *Clim. Change* **72** 251–98
[7] French N H F, Jenkins L K, Loboda T V, Flannigan M, Jandt R, Bourgeau-Chavez L L and Whitley M 2015 Fire in arctic tundra of Alaska: past fire activity, future fire potential, and significance for land management and ecology *Int. J. Wildland Fire* **24** 1045–61
[8] Rocha A V, Loranty M M, Higuera P E, Mack M C, Hu F S, Jones B M, Breen A L, Rastetter E B, Goetz S J and Shaver G R 2012 The footprint of Alaskan tundra fires during the past half-century: implications for surface properties and radiative forcing *Environ. Res. Lett.* **7** 044039
[9] Natali S M, Schuur E A G, Webb E E, Pries C E H and Crummer K G 2014 Permafrost degradation stimulates carbon loss from experimentally warmed tundra *Ecology* **95** 602–8
[10] Bret-Harte M S, Mack M C, Shaver G R, Huebner D C, Johnston M, Mojica C A and Reiskind J A 2013 The response of arctic vegetation and soils following an unusually severe tundra fire *Phil. Trans. R. Soc.* B **368** 20120490
[11] Grosse G *et al* 2011 Vulnerability of high-latitude soil organic carbon in North America to disturbance *J. Geophys. Res.* **116** G00K06
[12] Schuur E A G *et al* 2008 Vulnerability of permafrost carbon to climate change: implications for the global carbon cycle *BioScience* **58** 701–14
[13] Swanson F 1981 Fire and geomorphic processes *Fire Regime and Ecosystem Properties: Proceedings of the Conf. General Technical Report WO-GTR-26* (Washington, DC: US Department of Agriculture, Forest Service) pp 401–20
[14] Mackay J R 1995 Active layer changes (1968 to 1993) following the forest-tundra fire near Inuvik, NWT, Canada *Arctic Alpine Res.* **27** 323–36
[15] Shur Y L and Jorgenson M T 2007 Patterns of permafrost formation and degradation in relation to climate and ecosystems *Permafrost Periglacial Process.* **18** 7–19
[16] Brown D R N, Jorgenson M T, Douglas T A, Romanovsky V E, Kielland K, Hiemstra C, Euskirchen E S and Ruess R W 2015 Interactive effects of wildfire and climate on permafrost degradation in Alaskan lowland forests *J. Geophys. Res.* **120** 1619–37
[17] Liu L, Zhang T and Wahr J 2010 InSAR measurements of surface deformation over permafrost on the North Slope of Alaska *J. Geophys. Res.* **115** F03023
[18] Liu L, Schaefer K, Zhang T and Wahr J 2012 Estimating 1992–2000 average active layer thickness on the Alaskan North Slope from remotely sensed surface subsidence *J. Geophys. Res.* **117** F01005
[19] Schaefer K, Liu L, Parsekian A, Jafarov E, Chen A, Zhang T, Gusmeroli A, Panda S, Zebker H A and Schaefer T 2015 Remotely sensed active layer thickness (ReSALT) at Barrow, Alaska using interferometric synthetic aperture radar *Remote Sens.* **7** 3735–59
[20] Rosen P A, Hensley S, Joughin I R, Li F K, Madsen S N, Member S, Rodríguez E and Goldstein R M 2000 Synthetic aperture radar interferometry *Proc. IEEE* **88** 333–82
[21] Liu L, Jafarov E E, Schaefer K M, Jones B M, Zebker H A, Williams C A, Rogan J and Zhang T 2014 InSAR detects increase in surface subsidence caused by an Arctic tundra fire *Geophys. Res. Lett.* **41** 3906–13
[22] Iwahana G, Uchida M, Liu L, Gong W, Meyer F J, Guritz R, Yamanokuchi T and Hinzman L 2016 InSAR detection and field evidence for thermokarst after a tundra wildfire, using ALOS-PALSAR *Remote Sens.* **8** 218
[23] Burns J J 1964 Pingos in the Yukon–Kuskokwim delta, Alaska: their plant succession and use by mink *Arctic* **17** 203–10
[24] Péwé T L 1964 Ice wedges in Alaska-classification, distribution, and climatic significance *Geol. Soc. America Spec. Paper* **76** 129
[25] Zebker H A, Hensley S, Shanker P and Wortham C 2010 Geodetically accurate InSAR data processor *IEEE Trans. Geosci. Remote Sens.* **48** 4309–21
[26] Goldstein R M and Werner C L 1998 Radar interferogram filtering for geophysical applications *Geophys. Res. Lett.* **25** 4035–8
[27] Chen C W and Zebker H A 2002 Phase unwrapping for large SAR interferograms: statistical segmentation and generalized network models *IEEE Trans. Geosci. Remote Sens.* **40** 1709–19
[28] Chen J, Knight R and Zebker H A 2017 The temporal and spatial variability of the confined aquifer head and storage properties in the San Luis Valley, Colorado inferred from multiple InSAR missions *Water Resour. Res.* **53** 9708–20
[29] Hooper A 2008 A multi-temporal insar method incorporating both persistent scatterer and small baseline approaches *Geophys. Res. Lett.* **35** L16302
[30] Schmidt D A and Burgmann R 2003 Time-dependent land uplift and subsidence in the Santa Clara Valley, California, from a large interferometric synthetic aperture radar data set *J. Geophys. Res.* **108** 2416
[31] Lauknes T, Shanker A P, Dehls J, Zebker H, Henderson I and Larsen Y 2010 Detailed rockslide mapping in northern norway with small baseline and persistent scatterer interferometric SAR time series methods *Remote Sens. Environ.* **114** 2097–109
[32] Chen J, Zebker H A, Segall P and Miklius A 2014 The 2010 slow slip event and secular motion at Klauea, Hawaii, inferred from TerraSAR-X InSAR data *J. Geophys. Res.* **119** 6667–83
[33] Liu L, Schaefer K M, Chen A C, Gusmeroli A, Zebker H A and Zhang T 2015 Remote sensing measurements of thermokarst subsidence using InSAR *J. Geophys. Res.* **120** 1935–48
[34] French N H F, Whitley M A and Jenkins L K 2016 Fire disturbance effects on land surface albedo in Alaskan tundra *J. Geophys. Res.* **121** 841–54
[35] Ludwig S, Holmes R M, Natali S, Schade J and Mann P 2018 Yukon–Kuskokwim delta fire: soil and permafrost: bulk density, pH, soil organic matter, ice content, cryostratigraphy, and nutrient profiles, Yukon–Kuskokwim delta, Alaska, 2016 *Arctic Data Center* (https://doi.org/10.18739/A2KW57H4V)
[36] Parsekian A D, Slater L and Giménez D 2012 Application of ground-penetrating radar to measure near-saturation soil water content in peat soils *Water Resour. Res.* **48** W02533
[37] Chen A, Parsekian A D, Schaefer K, Jafarov E, Panda S, Liu L, Zhang T and Zebker H 2016 Ground-penetrating radar-derived measurements of active-layer thickness on the landscape scale with sparse calibration at Toolik and Happy Valley, Alaska *Geophysics* **81** H9–19

[38] Zwieback S, Hensley S and Hajnsek I 2015 Assessment of soil moisture effects on l-band radar interferometry *Remote Sens. Environ.* **164** 77–89
[39] Jorgenson T and Ely C 2001 Topography and flooding of coastal ecosystems on the Yukon–Kuskokwim delta, Alaska: implications for sea-level rise *J. Coast. Res.* **17** 124–36 (www.jstor.org/stable/4300157)
[40] Yufeng H, Lin L, Larson K M, Schaefer K M, Zhang J and Yao Y 2018 GPS interferometric reflectometry reveals cyclic elevation changes in thaw and freezing seasons in a permafrost area (Barrow, Alaska) *Geophys. Res. Lett.* **45** 5581–9
[41] Viereck L A and Schandelmeier L A 1980 Effects of fire in Alaska and adjacent Canada: a literature review *Technical Report 6* (Anchorage, AK: Bureau of Land Management, Alaska State Office)
[42] Schaefer K, Zhang T, Slater A G, Lu L, Etringer A and Baker I 2009 Improving simulated soil temperatures and soil freeze/thaw at high-latitude regions in the simple biosphere/Carnegie-Ames-Stanford approach model *J. Geophys. Res.* **114** F02021
[43] Loboda T, French N, Hight-Harf C, Jenkins L and Miller M 2013 Mapping fire extent and burn severity in Alaskan tussock tundra: an analysis of the spectral response of tundra vegetation to wildland fire *Remote Sens. Environ.* **134** 194–209
[44] Jenkins L K, Bourgeau-Chavez L L, French N H F, Loboda T V and Thelen B J 2014 Development of methods for detection and monitoring of fire disturbance in the Alaskan tundra using a two-decade long record of synthetic aperture radar satellite images *Remote Sens.* **6** 6347–64
[45] Jafarov E E, Romanovsky V E, Genet H, McGuire A D and Marchenko S S 2013 The effects of fire on the thermal stability of permafrost in lowland and upland black spruce forests of interior Alaska in a changing climate *Environ. Res. Lett.* **8** 035030